Research Paper

Metformin mitigates cisplatin-induced ovarian damage through inhibiting the pyroptosis of granulosa cells via ROS/TXNIP/NLRP3 signaling pathway

Bo Wang[1,2,3], Jian Li[4], Qianyu Zhang[1,2,3], Yuting Li[1,2,3], Wu Ren[1,2,3], Du He[5]

[1]Department of Obstetrics and Gynecology, Tongji Hospital, Tongji Medical College, Huazhong University of Science and Technology, Wuhan 430030, China
[2]National Clinical Research Center for Obstetrical and Gynecological Diseases, Wuhan 430030, China
[3]Key Laboratory of Cancer Invasion and Metastasis, Ministry of Education, Wuhan 430030, China
[4]Department of Hepatobiliary Surgery, Renmin Hospital of Wuhan University, Wuhan 430030, China
[5]Department of Medical Oncology, The Central Hospital of Enshi Tujia and Miao Autonomous Prefecture, Enshi 445000, China

Correspondence to: Du He; **email:** hdu1234@163.com, https://orcid.org/0000-0002-6358-3130
Keywords: ovarian damage, cisplatin, metformin, pyroptosis, ROS/TXNIP/NLRP3 pathway
Received: October 9, 2023 **Accepted:** January 29, 2024 **Published:** March 14, 2024

ABSTRACT

Cisplatin, a vital chemotherapy drug for solid malignant tumors, can detrimentally affect ovarian health and fertility in premenopausal patients with cancer. Currently, effective strategies to mitigate cisplatin-induced ovarian damage remain limited. Several studies have highlighted the potential of metformin as an anticancer agent with anti-aging properties and other health benefits. Hence, the present study established an animal model to investigate the impact of metformin on cisplatin-induced ovarian damage, elucidating its mechanisms using bulk RNA sequencing analysis and Western blotting. Our study findings demonstrate that metformin significantly prevents the decline in cisplatin-induced ovarian reserve, maintaining anti-müllerian hormone (AMH) and estradiol (E2) levels. Moreover, metformin may effectively improve cisplatin-induced ovarian fibrosis and granulosa cell pyroptosis through the ROS/TXNIP/NLRP3 pathway. In summary, our study indicates that metformin holds promise in alleviating cisplatin-induced ovarian damage, offering a potential avenue to preserve female fertility during chemotherapy.

INTRODUCTION

In recent years, there has been a global rise in cancer diagnosis among women, with an increasing trend in younger patients [1]. Consequently, there is a growing focus on safeguarding the ovarian endocrine and reproductive functions of female patients with cancer [2]. Cisplatin, a broad-spectrum anticancer drug used in the treatment of various malignancies, including head and neck squamous cell carcinoma, lymphosarcoma, ovarian cancer, and cervical cancer, exerts its therapeutic effects by inhibiting DNA replication and transcription within tumor cells [3]. However, alongside its anticancer properties, cisplatin unavoidably inflicts toxic effects, including nephrotoxicity, gastrointestinal toxicity, ototoxicity, cardiac toxicity, and ovarian toxicity, on the body [3–5]. Previous studies have confirmed that cisplatin damages the ovarian endocrine function, leading to hormonal imbalances and endocrine disorders [2, 5, 6]. In addition, it induces a reduction in ovarian primordial follicles, decreasing ovarian reserve and diminishing the number of sinusoidal follicles. These consequences result in decreased female fertility and potential infertility [2, 7–9]. Consequently, there is an urgent need to identify new preventive measures that can mitigate ovarian damage caused by chemotherapy

drugs without compromising chemotherapy efficacy to ensure the reproductive system development and fertility of childbearing-age female patients with cancer.

Metformin, a well-established first-line treatment for type 2 diabetes, boasts a lengthy history of clinical application [10]. Remarkably, it has shown promise in promoting ovulation in patients with polycystic ovary syndrome and reducing the risk of ovarian hyperstimulation syndrome during *in vitro* fertilization treatment [11, 12]. Hence, it is considered a potential candidate for reducing chemotherapy-induced ovarian toxicity [5, 13]. Beyond this, metformin has exhibited the ability to enhance the effectiveness of cisplatin chemotherapy while impeding the progression and metastasis of ovarian cancer [14, 15]. However, further exploration is necessary to determine whether metformin can effectively mitigate chemotherapy-induced ovarian toxicity and elucidate the underlying molecular mechanisms.

Thioredoxin interacting protein (TXNIP), a protein sensitive to oxidative stress, plays a crucial role in oxidative stress and the activation of inflammasomes associated with NOD-like receptor heat protein domain 3 (NLRP3) [16]. Inhibition of NLRP3 inflammasome activation has been shown to reduce cell death in various contexts, such as myocardial cells and human umbilical vein endothelial cells [17, 18]. A previous study showed that cell pyroptosis, a programmed cell death mode reliant on Caspase-1, is accompanied by the release of pro-inflammatory factors [19]. Gasdermin-D (GSDMD) protein is a key player in cell pyroptosis and can be activated by inflammatory Caspase cleavage, potentially leading to cell pyroptosis [19, 20]. Furthermore, cisplatin amplifies ovarian oxidative stress responses and elevates reactive oxygen species (ROS) levels within follicles [6, 21]. Ovarian granulosa cells, known as the "guardian" of oocytes, represent pivotal determinants of follicular development and are susceptible targets for ovarian damage induced by chemotherapy agents such as cisplatin [22]. Effective interventions and protective measures for these cells are currently lacking. It is postulated that cisplatin may accelerate ovarian granulosa cell apoptosis, promoting follicular atresia. However, the role of metformin in cisplatin-induced granulosa cell pyroptosis via the ROS/TXNIP/NLRP3 signaling pathway remains unclear. Therefore, the present study aims to establish an animal model of cisplatin-induced ovarian damage, investigating whether metformin mediates through the ROS/TXNIP/NLRP3 signaling pathway to regulate cisplatin-induced ovarian granulosa cell pyroptosis. These findings hold promise for advancing the prevention and treatment of chemotherapy-induced ovarian damage.

MATERIALS AND METHODS

Construction of cisplatin-induced ovarian damage model

C57BL/6J mice (age, 7 weeks) used in this study were provided by Speyford Biotechnology Co., Ltd. (Beijing, China). All mice were housed in a specific pathogen-free animal room with a controlled temperature (20–25° C), humidity (30%–70%), and light exposure cycle (12-h light–dark cycle), and the experimental period was one month. Mice were divided into three groups as follows: control (Con, N = 20), cisplatin (Cis, N = 20), and cisplatin plus metformin (Cis + Met, N = 20) groups. Cisplatin (Sigma, Z2125, USA) was dissolved in DMSO (40 mg/mL) and stored at -20° C in the dark.

Before intraperitoneal injection, cisplatin was thawed and dissolved in 0.9% normal saline. Mice in the Cis and Cis + Met groups were intraperitoneally injected with cisplatin at the age of 8 weeks. Mice in the Cis + Met group were orally administered metformin hydrochloride sustained-release tablets (C4H11N5•HCl) for thirty days according to their body weight. Metformin was dissolved in 0.9% normal saline and administered intragastrically.

Cell cultures and treatments

C57BL/6J female mice were euthanized by neck dissection, and their ovaries were removed and placed in sterile LPS solution. The fallopian tubes and adipose tissue around the ovaries were separated under a microscope, and a 1 mL syringe needle was used to puncture the ovaries to obtain granulosa cells. LPS containing granulosa cells was transferred to an EP tube, then the container was rinsed twice with McCoy's 5a culture medium and transferred to the EP tube. Centrifuge (800 rpm) for 5 minutes, resuspend with culture medium, and inoculate in a six well plate. Then, culture in a 37° C, 5% CO_2 incubator.

Reverse transcription and quantitative real-time polymerase chain reaction (qRT-PCR) analysis

Total RNA was extracted from mGCs and purified using the TRIzol reagent. The extracted RNA (1 μg) was reverse-transcribed into cDNA using HiScript II Q RT SuperMix for quantitative polymerase chain reaction (qPCR) (+gDNA eraser). Quantitative reverse transcription polymerase chain reaction (qRT-PCR) was performed in triplicate on a CFX96 real-time PCR system (Bio-Rad, USA). The final volume of the PCR reaction mixture was 20 μL. After amplification, dissociation curves were plotted to ensure the purity of the PCR product, and the gene expression levels were calculated using the $2^{\Delta\Delta Ct}$ method.

Enzyme-linked immunosorbent assay

The concentration of E2, follicle-stimulating hormone (FSH), and AMH in the serum of C57BL/6 mice was measured using commercial ELISA kits according to the manufacturer's instructions. Antigens were diluted in a coating diluent to an appropriate concentration, and 100 antigens per well microliter were added. The samples were incubated at 37° C for 4 h, then discarded the liquid in the hole, and the samples were sealed with 5% calf serum at 37° C for 40 min. The reaction holes were sealed with the sealing solution, and bubbles were removed from each hole. The holes were washed thrice with washing solution, each time for 3 minutes. The diluted sample was added to the enzyme-labeled reaction well. Each sample was added into at least two wells, 100 for each well microliter. The samples were incubated at 37° C for 40–60 min and washed as mentioned above. According to the reference working dilution provided by the enzyme conjugate provider, substrate was added: 100 per well microliter. The samples were incubated at 37° C for 3–5 minutes away from light, termination solution was added for color development (50 per well microliter), and analyzed within 20 min.

Hematoxylin-eosin (HE) staining and follicle counting

For hematoxylin and eosin (H&E) staining, the ovarian tissues of mice were embedded in paraffin and cut into 5-μm-thick sections. The tissue slices were mounted on glass microscope slides, air-dried at room temperature for 24 hours, and stored at room temperature. When preparing for use, the slides were dewaxed in xylene, rehydrated in a series of graded alcohols (100%, 95%, 80%, and 75%), and washed with distilled water. Rehydrated slices were first treated with hematoxylin until the required degree of staining was reached (Servicebio, Wuhan, China), washed with tap water to remove excess solution, differentiated in 1% acid alcohol for 30 seconds, and washed again with tap water for 60 seconds. The sections were counterstained with eosin and dehydrated using ethanol and 100% xylene.

Follicles were counted using H&E-stained ovarian sections as previously described. Follicles are divided into four types as follows: primordial, primary, secondary, and sinus follicles. The primordial follicle is characterized by a tight oocyte surrounded by a layer of flattened granulosa cell, whereas the primary follicle is characterized by an enlarged oocyte surrounded by a layer of cubic granulosa cell. Secondary follicles are defined as enlarged oocytes surrounded by at least a partial or complete second layer of cubic granulosa cell but no more than four layers of complete cubic granulosa cell. Sinus follicles are characterized by the presence of follicular fluid regions (sinuses) or a single large sinus cavity. If the oocytes degenerate (curl, concentrate, or fragment) or are lost, follicles in the primitive, primary, and preantral stages of development are considered atresia. In antral atretic follicles, the basement-separating oocytes from granulosa cell are often thickened into a vitreous membrane, and granulosa cell is replaced by fibrous substances. To avoid counting one follicle twice, the number of primordial, primary, and secondary follicles was counted once in every 5 consecutive sections, and the number of sinus follicles was counted once in every 40 consecutive sections. Follicular density was calculated by dividing the number of follicles by the analytical volume. Subsequently, the proportion of atretic follicles in total follicles (including healthy follicles and atretic follicles at each stage) was calculated.

Immunofluorescence

The ovaries of mice were made into paraffin sections, which were then dewaxed and antigen-repaired sequentially. Then, 3% BSA was added to the sections and incubated at room temperature for 30 minutes, followed by the addition of primary and secondary antibodies. Next, the slices were placed in PBS solution and continue shaking on the shaking table for 5 minutes. Then, DAPI staining solution was added to the slice and incubate it at room temperature in a dark place for approximately 10 minutes. The slices were placed in PBS and continue shaking on the shaking table for 5 minutes before sealing them. Finally, images were collected using an inverted fluorescence microscope for subsequent data analysis.

The ROS fluorescence operation steps mainly include the preparation of DCFH-DA probes (i.e. diluting with serum-free cell culture medium or Early's equilibrium salt solution (G4213) at a ratio of 1:1000 to prepare DCFH-DA working solution), loading probes, and ROS detection. Finally, observation and capturing of images were done using instruments such as fluorescence microscopy or confocal microscopy (with excitation wavelength of 488 nm and emission wavelength of 525nm set).

Transmission electron microscopy

After the fresh ovaries of mice were completely removed, a culture dish containing electron microscopy fixative was immediately filled. Then, the small groups of tissue blocks were removed *in vitro* and immediately placed into the culture dish. A surgical knife was used to cut them into small pieces in the fixative of the culture dish. Finally, after completing the negative staining of the slices, electron microscopy observation and photography were performed to obtain the field of view.

Masson staining and polarized light

The embedded paraffin sections were subjected to gradient dewaxing with xylene, anhydrous ethanol, 95%, and 75% ethanol until water was obtained. Then, they were stained with prepared Weigert iron hematoxylin solution for 8 minutes, differentiated with acidic ethanol solution for 15 seconds, and stained with Masson blue solution for 5 minutes, followed by staining with Lichun fuchsin staining solution for 5 minutes. Finally, they were treated with weak acid working solution, phosphomolybdic acid solution, and aniline blue staining solution for 1 minute, immediately after dehydration and transparent sealing with neutral gum, images were collected under an optical microscope. Collagen fibers, mucus, and cartilage were blue in color (such as bright green staining), cytoplasm was red, and nucleus was black blue.

Polarized light photography involves tissue sampling, embedding, paraffin sectioning, frozen sectioning, staining, turning on the polarized light microscope, CCD switch, flipping the polarizer, and opening the computer and microscope imaging software. Place the prepared stained sections on a white light microscope stage and secure them with a section clamp. Move the stage up, down, left, and right to align the tissue on the slice with the objective lens. Adjust the microscope light source to the appropriate brightness, observe the slices with an eyepiece, and find the tissue by coarse focusing under a low magnification objective. Adjust the microscope lever to both observation and imaging mode, and select an objective lens with an appropriate magnification for the microscope.

Terminal deoxynucleotidyl transferase-mediated dUTP-biotin nick end labelling (TUNEL) staining

Wash the paraffin sections sequentially with xylene, gradient ethanol, and PBS, then mix well with 50 ul TdT and 450 ul dUTP solution labeled with fluorescein. For the negative control group, only 50 ul of fluorescein labeled dUTP solution was added, while for the positive control group, 100 ul DNase1 was added first, and the reaction was carried out at 15-25° C for 10 minutes. After the glass slides were dried, carefully remove the excess liquid around the sections with filter paper, and add 50 ul TUNEL reaction mixture (for the negative control group, only 50 ul of fluorescein labeled dUTP solution was added). Cover the specimen with a glass slide or sealing film and react in a dark wet box at 37° C for 1 hour. Then add to the pre heated washing and termination reaction buffer at 37° C, keep at 37° C for 30 minutes, rinse with PBS three times, dry the glass slide and add 50 ul of DIG-POD dry sample, cover with glass slide or sealing film, and react at 37° C for 30 minutes in a dark leak box. Rinse with PBS three times; re-dye with hematoxylin or methyl green, and rinse immediately with tap water after a few seconds. Gradient alcohol dehydration, xylene transparency, and neutral gum sealing were used to obtain images through photography.

Western blot analysis

After isolating C57BL/6J mouse ovaries or granulosa cells cultured *in vitro*, an appropriate volume of RIPA lysis solution was added. Subsequently, granulosa cells or ovarian tissues were further lysed using ultrasound. The lysates were then centrifuged at 12000 rpm for 20 min at 4° C using a low-temperature, high-speed centrifuge. Under dark conditions, Coomassie Brilliant Blue and double distilled water were added for absorbance measurements, determining protein concentration using a multifunctional enzyme-linked immunosorbent assay at a wavelength of 595 nm.

Following this, a loading buffer was added to the protein samples, which were heated in a microwave at high heat until boiling and cooked at medium heat for 15 min to ensure protein denaturation. Subsequently, the protein electrophoresis gel was prepared and fixed in an electrophoresis tank. The electrophoresis solution was poured into the tank, after which 5 μL of protein markers and the corresponding volume of protein samples were added for each group. The transfer buffer was mixed with 800 mL of double-distilled water and 200 mL of methanol. The filter paper, electrophoresis gel, and PVDF film were placed in the transfer tank, and the transfer buffer was added over 100 min for continuous transfer. Next, BSA and TBST were mixed to create a sealing solution. The PVDF film was immersed in the solution and sealed at room temperature for 1 h. Subsequently, the first and second antibodies were incubated. The strips were immersed in an exposure solution using an ECL exposure solution, and the image was exposed and analyzed using the BioRad ChemiDoc MP gel imaging system.

Statistical analysis

The R language (version 4.0.2, https://www.r-project.org/) and GraphPad Prism (version 8.0.1) tools were used in this study. The econometric data were represented as mean ± standard deviation. Multiple group comparisons were conducted using one-way ANOVA, followed by pairwise comparisons between the two groups using the SNK-q test. $P < 0.05$ was considered statistically significant.

RESULTS

Cisplatin-induced ovarian endocrine dysfunction was alleviated by metformin

Three groups of 7-week-old mice (equivalent to humans aged 20–30 years) were randomly assigned: a blank control group, a cisplatin group (5 mg/kg, 8-week-old), and a cisplatin+metformin (250 mg/kg) intervention group. The cisplatin-exposed mice were either continuously given metformin in their drinking water or not for a month to prevent and reverse cisplatin-induced acute ovarian injury (Figure 1A). To assess the impact of metformin and cisplatin on ovarian function, estrus cycles and hormone levels in the mice were examined, as these parameters are indicative of ovarian endocrine function. As shown in Figure 1B–1E, disruptions in the estrous cycles were initiated in the cisplatin group after one week of exposure to cisplatin, with a normal estrous cycle proportion of 33.33% compared to 86.67% ($P < 0.05$) in the control group. Interestingly, estrous cycle disturbances were also observed in mice receiving metformin water. However, after two weeks of cisplatin exposure, the proportion of mice with restored normal estrous cycle reached 60.00% in the metformin group, whereas it remained at 26.67% ($P < 0.05$) in the cisplatin group. Consistent with these findings, the E2 levels in the metformin group were significantly higher than those in the cisplatin-exposed group, while FSH levels in the metformin group were lower than those in the cisplatin group ($P < 0.05$). However, there was no significant difference in AMH levels between the two groups ($P < 0.05$) (Figure 1F–1H). Hence, these results indicate that metformin can potentially reverse cisplatin-induced ovarian endocrine dysfunction in mice.

Cisplatin-induced ovarian reserve depletion was mitigated by metformin

To further investigate the impact of metformin on ovarian function in cisplatin-exposed mice, ovarian histological analysis was conducted. As shown in Figure 2A–2G, the follicle count serves as a direct indicator of ovarian reserve capacity. In this study, it was observed that in the ovaries of cisplatin-exposed mice, there was a significant reduction in the number of primordial and growing follicles, along with a substantial increase in atretic follicles compared to the control group ($P < 0.05$). It is noteworthy that metformin treatment was associated with the optimization of ovarian reserve preservation and the mitigation of cisplatin-induced follicular atresia. In summary, the ovaries of cisplatin-exposed mice suffered severe damage to their reserve and function, which was effectively reversed by metformin treatment.

Cisplatin-induced ovarian fibrosis was attenuated by metformin

Ovarian fibrosis is known as the leading cause of various ovarian dysfunctions. In this study, we assessed the potential of metformin in reversing ovarian fibrosis in cisplatin-exposed mice using Masson staining (Figure 3A). Quantification of ovarian fibrosis revealed a significant increase in fibrosis levels in cisplatin-exposed mice. Remarkably, metformin treatment demonstrated a substantial capacity to alleviate ovarian fibrosis in cisplatin-exposed mice ($P < 0.05$). Polarized light imaging analysis using Masson staining showed that metformin intervention resulted in a weakened fibrosis imaging signal in the ovarian interstitial area of cisplatin-exposed mice, aligning closely with the Sirius red staining results (Figure 3B, 3C). Furthermore, the number of granulosa cell apoptosis significantly increased within the follicles of cisplatin-exposed mice (Figure 3D). However, metformin intervention effectively reversed the heightened granulosa cell apoptosis ($P < 0.05$). In summary, the findings indicate that cisplatin exerts a potent acute destructive and toxic impact on ovarian structure and granulosa cells, and metformin counteracts cisplatin-induced ovarian fibrosis and mitigates the loss of granulosa cell apoptosis.

Cisplatin-induced acute ovarian injury via oxidative stress was alleviated by metformin

To explore the potential mechanisms underlying metformin's reversal of ovarian damage in cisplatin-exposed mice, bulk sequencing was conducted on ovarian tissues from the control, metformin intervention, and cisplatin-exposed groups. The results revealed a significant upregulation of pathways associated with oxidative stress signals in ovarian tissues of cisplatin-exposed mice compared to the control group ($P < 0.05$). However, metformin intervention led to a downregulation of these pathways (Figure 4A, 4B). Consistent with the sequencing findings, a notable enhancement of ROS fluorescence signals was observed in the ovarian tissues of cisplatin-exposed mice compared to the control group, while the metformin group exhibited a downward trend of ROS expression ($P < 0.05$) (Figure 4C, 4D). Furthermore, the expression of oxidative stress-sensitive proteins, TXNIP and NLRP3, significantly increased in the cisplatin group compared to the control group (Figure 4E, 4F). Conversely, the expression of TXNIP and NLRP3 proteins in the metformin intervention group showed a significant downward trend compared to the cisplatin group ($P < 0.05$). These findings suggest that metformin may reverse acute ovarian injury in cisplatin-exposed mice through an inflammatory signaling pathway modulation linked to oxidative stress.

Cisplatin-induced granular cell pyroptosis was alleviated by metformin via the ROS/TXNIP/NLRP3 axis

Previous studies indicated that cisplatin exposure leads to ROS accumulation in the ovaries, exacerbating acute ovarian injury and potentially involving the TXNIP/NLRP3 signaling pathway. Consistent with previous research reports, the release of pro-inflammatory factors such as IL-1β and TNF-α triggers cell apoptosis. We further investigate the occurrence of ovarian granulosa cell pyroptosis in cisplatin-exposed mice, the number of pyroptotic cells in the cisplatin-exposed group significantly increased compared to the control group

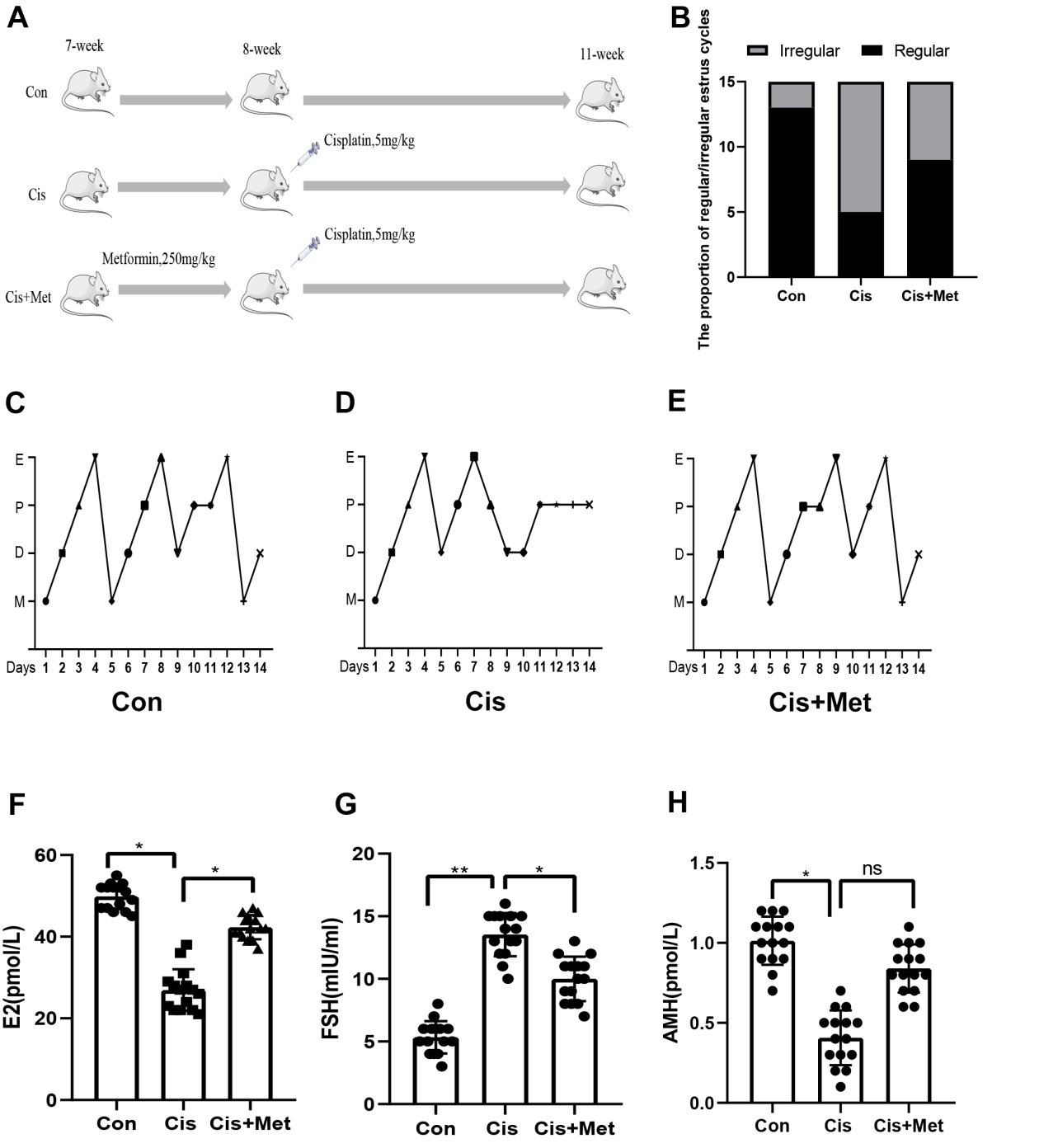

Figure 1. Reversal of cisplatin-induced ovarian dysfunction and estrous cycle by metformin. (**A**) Schematic description of the experimental design. (**B**) Percentage of regular and irregular estrous cycles in each group (N=15). (**C**–**E**) Estrous cycle of each group. (**F**–**H**) Serum E2, FSH and AMH of following the administration of each group. *p < 0.05, **p < 0.01, ***p < 0.001.

(P < 0.05), while the number of granulosa cell pyroptosis significantly decreased in the metformin intervention group (P < 0.05) (Figure 5A–5C). Consistent with these observations, granulosa cells in the cisplatin group exhibited significant upregulation in the protein expression levels of Caspase-1, GSDMD, IL-1β, and TNF-α (P < 0.05), while IL-1β and TNF-α showed significant downregulation in the metformin intervention group compared to the control group (P < 0.05) (Figure 5D–5F). In addition, as shown in Figure 5G, 5H, changes in the number of granulosa cell pyroptosis after co intervention with TXNIP inhibitor (SRI-37330) and metformin was not statistically significant (P>0.05) compared to metformin rescue. These findings suggest

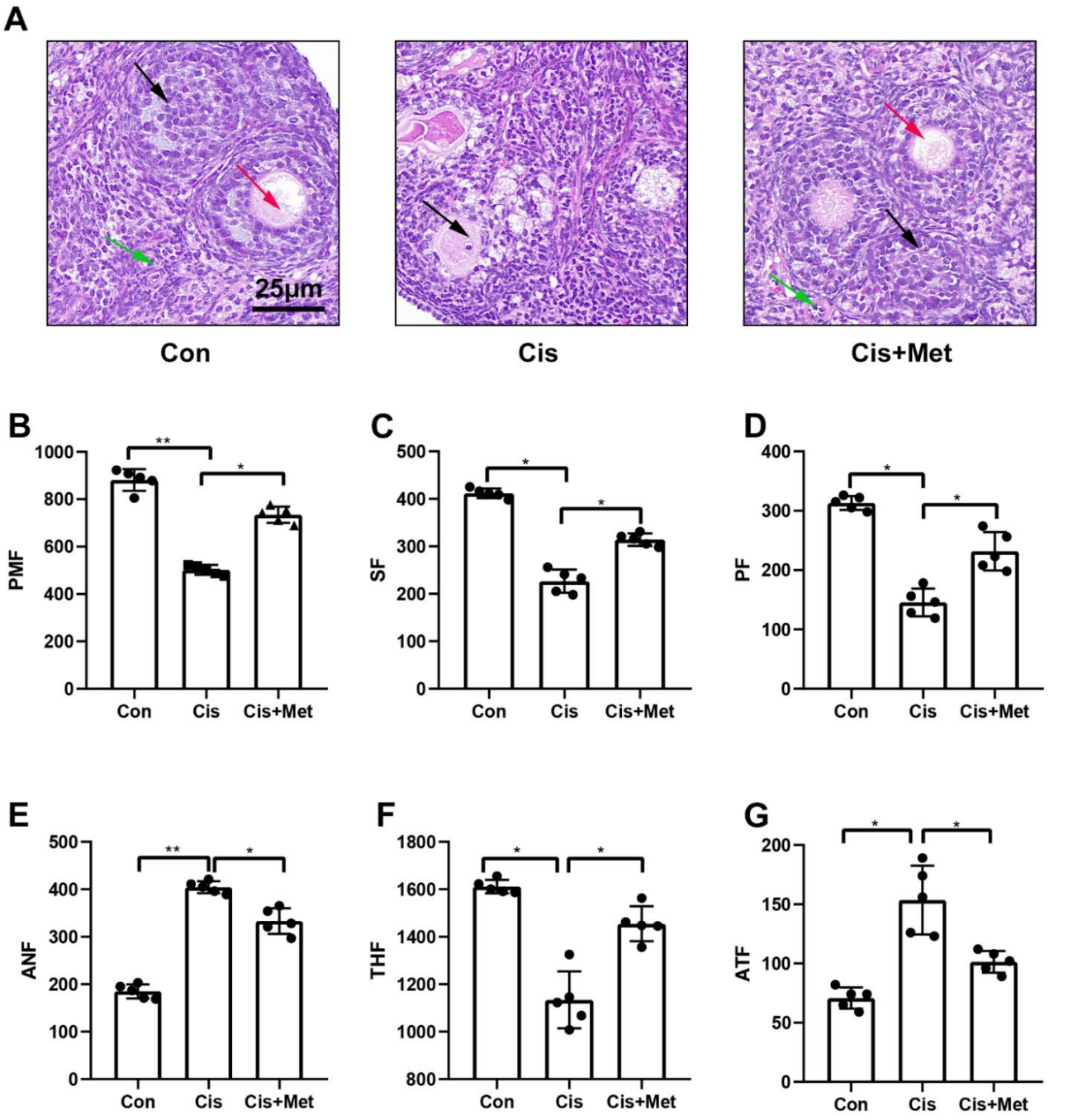

Figure 2. Reversal of cisplatin ovarian follicular loss at all levels by metformin. (**A**) HE staining of ovarian sections (×400). (**B**–**G**) Quantitative counting of follicles at different levels (n =5). PMF: primordial follicles (green line); PF: primary follicles; SF: secondary follicles; ANF: antral follicles; THF: total heathy follicles; ATF: atretic follicles (black line). Growing follicles (PF, SF, ANF, red line) *p < 0.05, **p < 0.01, ***p < 0.001.

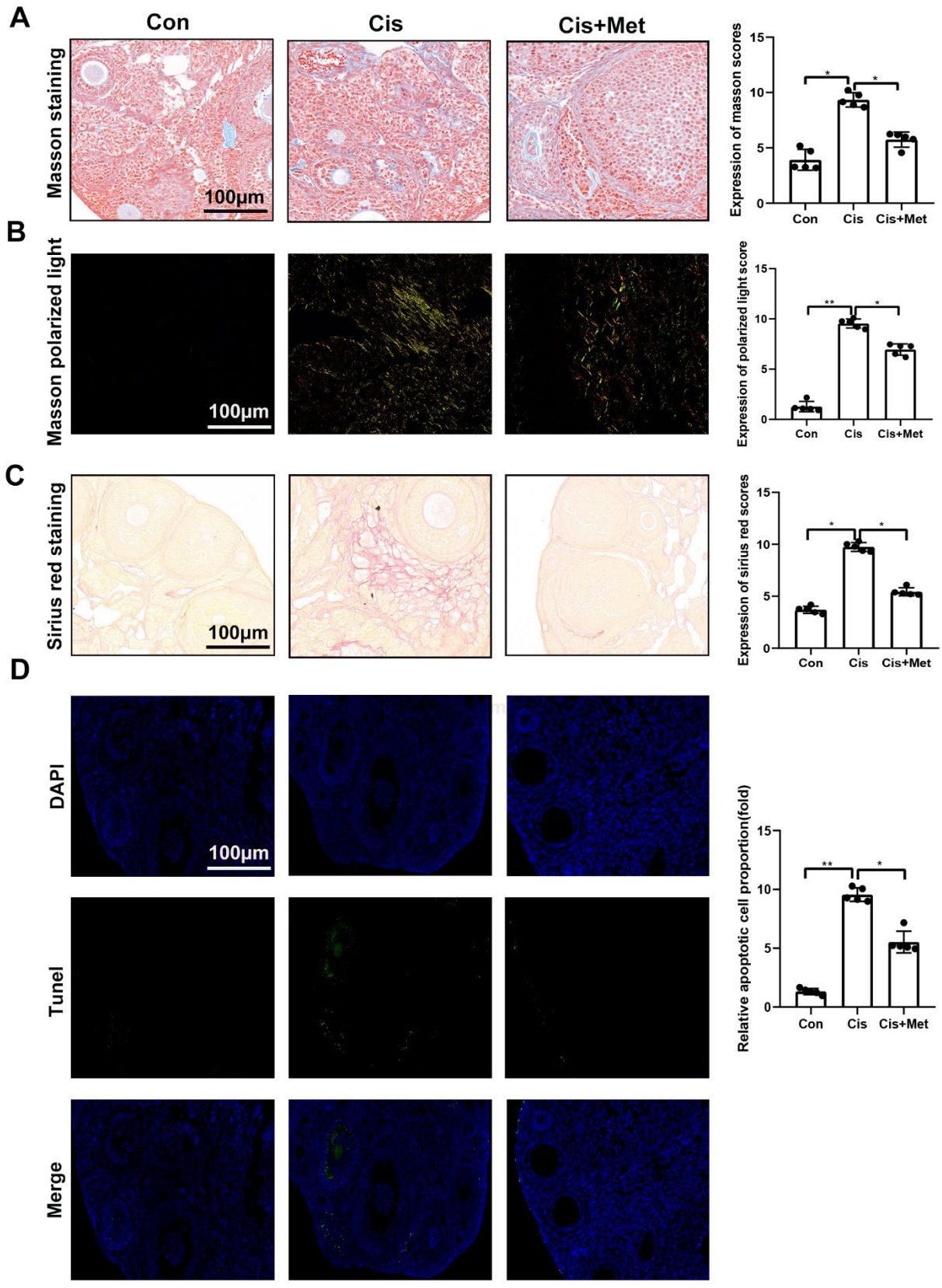

Figure 3. Reversal of cisplatin-induced ovarian fibrosis and granulosa cell apoptosis by metformin. (**A**, **B**) Representative images of Masson-stained ovaries and polarized light (×100). (**C**) Representative images of Sirius red stained ovaries (×100). (**D**) Immunofluorescence of TUNEL after treatment in each group (×100). *p < 0.05, **p < 0.01, ***p < 0.001.

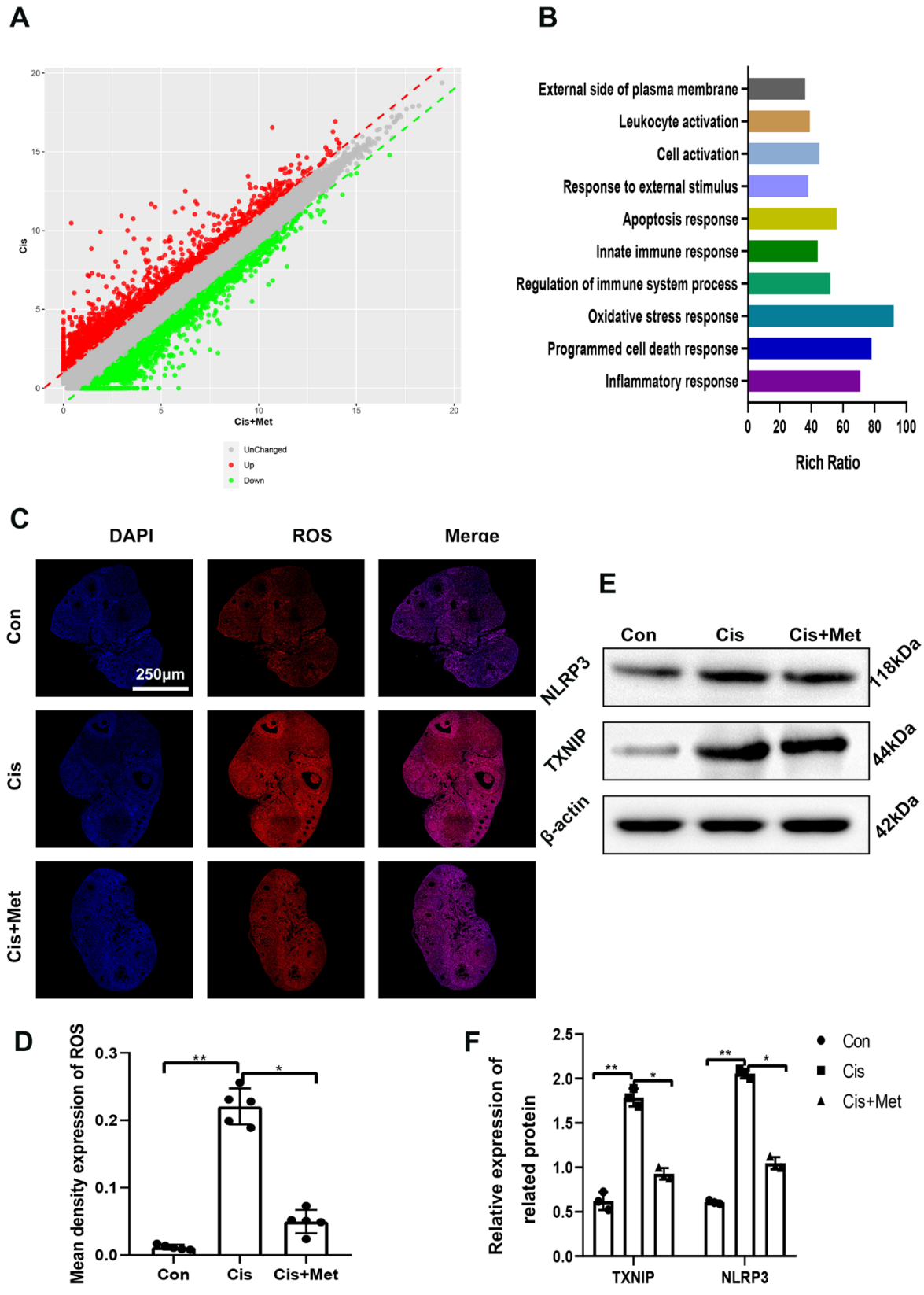

Figure 4. Reversal of cisplatin-induced acute ovarian damage by metformin. (**A**) Bulk sequencing reveals genes significantly upregulated or downregulated by metformin in alleviating ovarian damage. (**B**) GO terms enriched based on DEGs between the Cis group and Cis+Met groups. (**C**, **D**) Immunofluorescence of ROS after treatment in each group (×40). (**E**, **F**) Western blot analysis of NLRP3 and TXNIP protein expressions in ovaries treated with different medication regimens. *p < 0.05, **p < 0.01, ***p < 0.001.

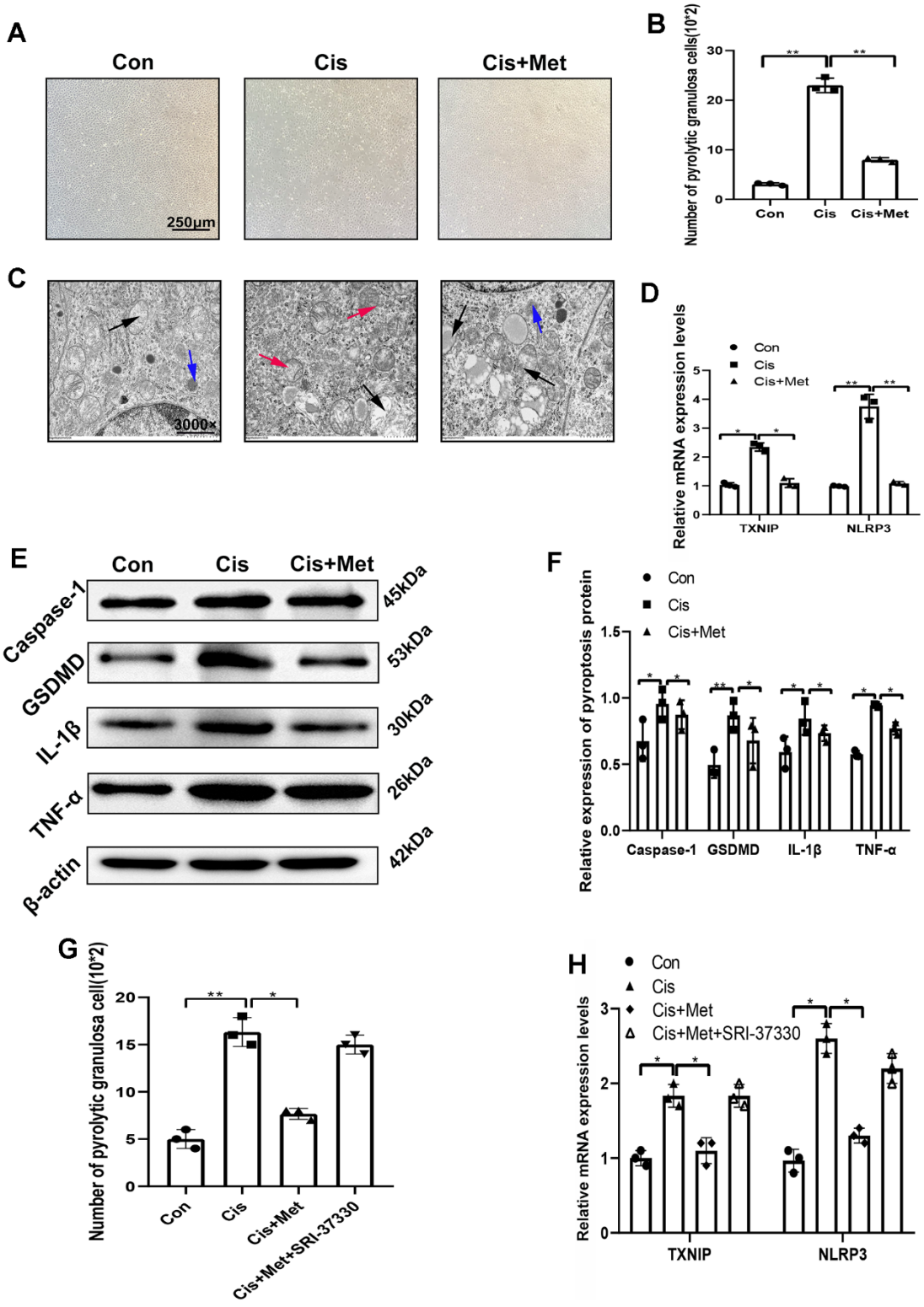

Figure 5. Reversal of cisplatin-induced granular cell pyroptosis by metformin. (**A**, **B**) Percentage of granulosa cell proliferation and pyroptosis in each group. (**C**) Transmission electron microscopy images showed subcellular morphology of mouse ovaries treated with different methods (cisplatin or metformin). Notes: Black arrow: mitochondria; Blue arrow: endoplasmic reticulum; Red arrow: nucleus of the granular cell. (**D**) Real-time PCR quantitative analysis of the expression levels of oxidative stress related genes in each group. (**E**, **F**) Western blot analysis of Caspase-1, GSDMD, IL-1β, and TNF-α protein expressions in ovaries treated with different medication regimens. *$p < 0.05$, **$p < 0.01$. (**G**) Comparison of the number of granulosa cell pyroptosis after different intervention methods. (**H**) Changes in gene expression of granulosa cell inflammation after different intervention methods.

that metformin inhibits ROS levels in ovarian granulosa cells exposed to cisplatin, potentially by inhibition of the TXNIP/NLRP3 signaling pathway. This, in turn, promotes cell proliferation and reduces the occurrence of granulosa cell pyroptosis.

DISCUSSION

As treatment options diversify, cancer survivors often experience significantly extended lifespans, sparking concerns about post-treatment quality of life. Generally, chemotherapy drugs are used to target the high proliferative capacity characteristic of cancer cells [2]. Unfortunately, they can also cause damage to healthy tissues, resulting in cardiac toxicity, gastrointestinal adverse reactions, nephrotoxicity, peripheral neurotoxicity, and ovarian toxicity [2, 23]. Among these, ovarian toxicity is a major side effect of therapeutic chemotherapy, impacting a significant portion of female patients with cancer [2]. Long-term chemotherapy-induced ovarian damage encompasses various issues, including but not limited to reduced ovarian reserve, infertility, and ovarian atrophy [2, 24]. Therefore, investigating the underlying mechanisms of chemotherapy-induced ovarian damage holds promise for the development of protective adjuvants to safeguard reproductive health in female patients undergoing routine cancer treatment.

In this study, a comprehensive set of *in vitro* and *in vivo* experiments were executed to confirm the side effects of conventional chemotherapy drugs on ovarian morphology and function. These experiments aimed to underscore the evidence and elucidate potential mechanisms behind cisplatin-induced ovarian dysfunction. Based on the previous studies, our findings confirm that cisplatin treatment significantly reduced the number of follicles across all developmental stages, with the absence of mature follicles. Subsequent examinations showed that the chemotherapy drugs used in this study significantly exacerbated ovarian fibrosis, stimulated ovarian cell apoptosis, reduced ovarian receptivity, and caused ovarian damage (morphological abnormalities and functional impairments). As expected, cisplatin treatment significantly reduced ovarian volume and the count of primordial and antral follicles within the ovaries of mice. Subsequently, a series of functional experiments were conducted to verify their toxic effects on ovarian fibrosis, apoptosis, receptivity, and function.

Subsequently, cisplatin treatment was observed to induce ovarian granulosa cell pyroptosis, likely stemming from oxidative damage and impaired antioxidant capacity induced by excessive ROS production. In addition, further experiments showed that cisplatin treatment significantly increased ROS levels. ROS overexpression serves as a pivotal trigger for cellular oxidative stress, which can cause dysfunctions such as metabolic damage, signal transduction changes, and inflammatory reactions and lead to cell apoptosis or pyroptosis. The present study is the first documentation of cisplatin-induced ovarian granulosa cell pyroptosis. In addition, metformin treatment alleviated cisplatin-induced granulosa cell toxicity by downregulating cellular ROS levels and enhancing antioxidant capacity.

Previous studies have shown that cell pyroptosis represents a programmed cell death mode reliant on Caspase-1, accompanied by the release of pro-inflammatory factors such as IL-1β and TNF-α [25]. Notably, the GSDMD protein is a key protein in cell pyroptosis, activated by inflammatory Caspase lysis to promote cell pyroptosis [26, 27]. The present study found that the addition of metformin significantly reduced the number of granulosa cell death, Caspase-1, GSDMD, IL-1β, and TNF-α compared with the cisplatin group, indicating a close association between the ROS/TXNIP/NLRP3 signaling pathway and cisplatin-induced granulosa cell pyroptosis. Previous studies have shown that TXNIP, as an oxidative stress sensitive protein, plays a crucial role in oxidative stress and NLRP3 inflammasome activation [28, 29]. As one of the important signaling pathways in inflammatory response, the TXNIP/NLRP3 signaling pathway is involved in the occurrence and development of various diseases, thereby activating the inflammatory cytokine mediated inflammatory response in the body. In addition, cell pyroptosis depends on the release of pro-inflammatory factors, among which the key protein GSDMD can be activated by inflammatory Caspase lysis, leading to cell pyroptosis. Consistent with previous studies, the inflammatory response and oxidative stress triggered by chemotherapy play significant roles in the occurrence and development of acute ovarian injury [21, 24, 30]. Therefore, it is speculated that inhibiting ROS levels could mitigate oxidative damage and the secretion of inflammatory factors induced by cisplatin within follicles and granulosa cells through the TXNIP/NLRP3 activation level modulation. This modulation may help hinder the advancement of chemotherapy-induced acute ovarian injury. To explore the potential outcomes of cell death resulting from chemotherapy-induced oxidative stress, we conducted RNA sequencing on ovarian tissues of mice from the control, cisplatin, and metformin intervention groups. Interestingly, the RNA-seq results suggest that cisplatin-induced ovarian damage may be attributed to oxidative stress, which is closely associated with excessive ROS production, despite some studies confirming a correlation between pyroptosis and chemotherapy-induced programmed cell death.

Granulosa cells play a crucial role in follicular development and maturation. Serving as an indispensable component of the ovary, these cells enveloping oocytes undergo periodic morphological changes, transitioning from a planar to a three-dimensional arrangement and from single-layer to multi-layer cells. Throughout the reproductive cycle, oocytes secreted by growth follicles and steroid hormones maintain the microenvironment of oocytes and promote follicular development, oocyte maturation, and ovulation [31]. Therefore, any damage to ovarian granulosa cells can result in oocyte death, follicular atresia, menstrual leakage, and even amenorrhea, which can detrimentally impact reproductive function. Consistent with previous studies, chemotherapy drugs may directly inhibit the proliferative abilities of granulosa cells during follicular development, leading to follicular atresia and subsequently triggering the premature activation of primordial and early depletion of the follicular pool [2, 24]. In addition, chemotherapy-induced ovarian damage can manifest through various mechanisms, primarily characterized by, but not limited to, growing follicular atresia, overactivation of primordial follicles, interstitial fibrosis, and acute ovarian vascular toxicity.

Pyroptosis, a recently recognized form of cell death, is characterized by programmed cell death, potentially mediated through the activation of the NLRP3/Caspase-1 signaling pathway triggered by oxidative stress. Research has shown that when cells undergo oxidative stress, they can induce and activate the release of the NLRP3 inflammasome, subsequently activating Caspase-1 and leading to the maturation of pro-inflammatory cytokines. This cascade, once initiated, leads to pyroptosis, resulting in the excessive release of pro-inflammatory cytokines and consequential tissue damage [32]. Our findings suggest that metformin may reverse cisplatin-induced pyroptosis and apoptosis in ovarian granulosa cells through the ROS/TXNIP/NLRP3 signaling pathway modulation triggered by oxidative stress. In addition, exposure to cisplatin chemotherapy has adverse effects on the ovaries and may be a potential risk factor for reduced ovarian function in women. Thus, our study offers fresh insights into the reproductive toxicity of cisplatin in females.

CONCLUSIONS

In summary, our study indicates that long-term exposure to cisplatin can induce granulosa cell pyroptosis through excessive oxidative stress, leading to reduced ovarian reserve. Furthermore, metformin can regulate ovarian granulosa cell pyroptosis to mitigate cisplatin-induced ovarian damage via the ROS/TXNIP/NLRP3 signaling pathway. These findings provide alternative prevention and treatment strategies for cisplatin-induced ovarian damage, as well as potential new targets for chemotherapy-induced ovarian damage protection.

AUTHOR CONTRIBUTIONS

Du He and Wu Ren are the co-corresponding authors of this article and designed the experiments. Bo Wang and Jian Li accomplished the molecular-biological experiments *in vitro*, *in vivo* and share the first co-authorship. Bo Wang, Qianyu Zhang and Yuting Li took the responsibility of animal drug administration and data analysis. All authors have revised the manuscript and agreed to publish it publicly.

CONFLICTS OF INTEREST

The authors declare no conflicts of interest.

ETHICAL STATEMENT

All experimental procedures were conducted in strict compliance with the Animal Care and Use Committee of Tongji Hospital, Tongji Medical College, Huazhong University of Science and Technology (IACUC Number: 2840).

FUNDING

This study has received funding from the Hubei Province Youth Talent Project (Project ID: WJ2021Q019).

REFERENCES

1. Sung H, Ferlay J, Siegel RL, Laversanne M, Soerjomataram I, Jemal A, Bray F. Global Cancer Statistics 2020: GLOBOCAN Estimates of Incidence and Mortality Worldwide for 36 Cancers in 185 Countries. CA Cancer J Clin. 2021; 71:209–49. https://doi.org/10.3322/caac.21660 PMID:33538338

2. Spears N, Lopes F, Stefansdottir A, Rossi V, De Felici M, Anderson RA, Klinger FG. Ovarian damage from chemotherapy and current approaches to its protection. Hum Reprod Update. 2019; 25:673–93. https://doi.org/10.1093/humupd/dmz027 PMID:31600388

3. Dasari S, Tchounwou PB. Cisplatin in cancer therapy: molecular mechanisms of action. Eur J Pharmacol. 2014; 740:364–78. https://doi.org/10.1016/j.ejphar.2014.07.025 PMID:25058905

4. Demkow U, Stelmaszczyk-Emmel A. Cardiotoxicity of

cisplatin-based chemotherapy in advanced non-small cell lung cancer patients. Respir Physiol Neurobiol. 2013; 187:64–7. https://doi.org/10.1016/j.resp.2013.03.013 PMID:23548823

5. Du D, Tang X, Li Y, Gao Y, Chen R, Chen Q, Wen J, Wu T, Zhang Y, Lu H, Zhang J, Wang S. Senotherapy Protects against Cisplatin-Induced Ovarian Injury by Removing Senescent Cells and Alleviating DNA Damage. Oxid Med Cell Longev. 2022; 2022:9144644. https://doi.org/10.1155/2022/9144644 PMID:35693700

6. Al-Shahat A, Hulail MA, Soliman NM, Khamis T, Fericean LM, Arisha AH, Moawad RS. Melatonin Mitigates Cisplatin-Induced Ovarian Dysfunction via Altering Steroidogenesis, Inflammation, Apoptosis, Oxidative Stress, and PTEN/PI3K/Akt/mTOR/AMPK Signaling Pathway in Female Rats. Pharmaceutics. 2022; 14:2769. https://doi.org/10.3390/pharmaceutics14122769 PMID:36559263

7. Ozyurt R, Celik N, Suleyman Z, Cagiran F, Kali Z, Gurkan N, Altindag F, Bulut S, Sarigul C, Dinc K, Suleyman H. Fertility protective effect of taxifolin in cisplatin-induced ovarian damage. Eur Rev Med Pharmacol Sci. 2022; 26:7195–203. https://doi.org/10.26355/eurrev_202210_29909 PMID:36263529

8. Huang J, Shan W, Li N, Zhou B, Guo E, Xia M, Lu H, Wu Y, Chen J, Wang B, Xi L, Ma D, Chen G, et al. Melatonin provides protection against cisplatin-induced ovarian damage and loss of fertility in mice. Reprod Biomed Online. 2021; 42:505–19. https://doi.org/10.1016/j.rbmo.2020.10.001 PMID:33388265

9. Yeh J, Kim BS, Liang YJ, Peresie J. Gonadotropin stimulation as a challenge to calibrate cisplatin induced ovarian damage in the female rat. Reprod Toxicol. 2009; 28:556–62. https://doi.org/10.1016/j.reprotox.2009.08.003 PMID:19737607

10. Sanchez-Rangel E, Inzucchi SE. Metformin: clinical use in type 2 diabetes. Diabetologia. 2017; 60:1586–93. https://doi.org/10.1007/s00125-017-4336-x PMID:28770321

11. Duan X, Zhou M, Zhou G, Zhu Q, Li W. Effect of metformin on adiponectin in PCOS: A meta-analysis and a systematic review. Eur J Obstet Gynecol Reprod Biol. 2021; 267:61–7. https://doi.org/10.1016/j.ejogrb.2021.10.022 PMID:34717078

12. Mourad S, Brown J, Farquhar C. Interventions for the prevention of OHSS in ART cycles: an overview of Cochrane reviews. Cochrane Database Syst Rev. 2017; 1:CD012103. https://doi.org/10.1002/14651858.CD012103.pub2 PMID:28111738

13. Qin X, Du D, Chen Q, Wu M, Wu T, Wen J, Jin Y, Zhang J, Wang S. Metformin prevents murine ovarian aging. Aging (Albany NY). 2019; 11:3785–94. https://doi.org/10.18632/aging.102016 PMID:31182682

14. Urpilainen E, Puistola U, Boussios S, Karihtala P. Metformin and ovarian cancer: the evidence. Ann Transl Med. 2020; 8:1711. https://doi.org/10.21037/atm-20-1060 PMID:33490223

15. Tossetta G. Metformin Improves Ovarian Cancer Sensitivity to Paclitaxel and Platinum-Based Drugs: A Review of *In Vitro* Findings. Int J Mol Sci. 2022; 23:12893. https://doi.org/10.3390/ijms232112893 PMID:36361682

16. Zhou R, Tardivel A, Thorens B, Choi I, Tschopp J. Thioredoxin-interacting protein links oxidative stress to inflammasome activation. Nat Immunol. 2010; 11:136–40. https://doi.org/10.1038/ni.1831 PMID:20023662

17. Huang Y, Xu W, Zhou R. NLRP3 inflammasome activation and cell death. Cell Mol Immunol. 2021; 18:2114–27. https://doi.org/10.1038/s41423-021-00740-6 PMID:34321623

18. Faria SS, Costantini S, de Lima VC, de Andrade VP, Rialland M, Cedric R, Budillon A, Magalhães KG. NLRP3 inflammasome-mediated cytokine production and pyroptosis cell death in breast cancer. J Biomed Sci. 2021; 28:26. https://doi.org/10.1186/s12929-021-00724-8 PMID:33840390

19. Li S, Sun Y, Song M, Song Y, Fang Y, Zhang Q, Li X, Song N, Ding J, Lu M, Hu G. NLRP3/caspase-1/GSDMD-mediated pyroptosis exerts a crucial role in astrocyte pathological injury in mouse model of depression. JCI Insight. 2021; 6:e146852. https://doi.org/10.1172/jci.insight.146852 PMID:34877938

20. Shi J, Gao W, Shao F. Pyroptosis: Gasdermin-Mediated Programmed Necrotic Cell Death. Trends Biochem Sci. 2017; 42:245–54. https://doi.org/10.1016/j.tibs.2016.10.004 PMID:27932073

21. Ayres LS, Berger M, Durli IC, Kuhl CP, Terraciano PB, Garcez TN, Dos Santos BG, Guimarães JA, Passos EP,

Cirne-Lima EO. Kallikrein-kinin system and oxidative stress in cisplatin-induced ovarian toxicity. Reprod Toxicol. 2020; 93:1–9. https://doi.org/10.1016/j.reprotox.2019.12.002 PMID:31874189

22. Chatterjee R, Helal M, Mobberley M, Ryder T, Bajoria R. Impaired steroidogenesis and apoptosis of granulosa-luteal cells in primary culture induced by cis-platinum. Am J Obstet Gynecol. 2014; 210:252.e1–7. https://doi.org/10.1016/j.ajog.2013.11.014 PMID:24215857

23. Ikesue H, Ishida M, Uchida M, Harada M, Haro T, Mishima K, Itoh Y, Kotsubo K, Yoshikawa M, Oishi R. Monitoring for potential adverse drug reactions in patients receiving chemotherapy. Am J Health Syst Pharm. 2004; 61:2366. https://doi.org/10.1093/ajhp/61.22.2366 PMID:15581259

24. Kim S, Kim SW, Han SJ, Lee S, Park HT, Song JY, Kim T. Molecular Mechanism and Prevention Strategy of Chemotherapy- and Radiotherapy-Induced Ovarian Damage. Int J Mol Sci. 2021; 22:7484. https://doi.org/10.3390/ijms22147484 PMID:34299104

25. Hsu SK, Li CY, Lin IL, Syue WJ, Chen YF, Cheng KC, Teng YN, Lin YH, Yen CH, Chiu CC. Inflammation-related pyroptosis, a novel programmed cell death pathway, and its crosstalk with immune therapy in cancer treatment. Theranostics. 2021; 11:8813–35. https://doi.org/10.7150/thno.62521 PMID:34522213

26. Tan Y, Chen Q, Li X, Zeng Z, Xiong W, Li G, Li X, Yang J, Xiang B, Yi M. Pyroptosis: a new paradigm of cell death for fighting against cancer. J Exp Clin Cancer Res. 2021; 40:153. https://doi.org/10.1186/s13046-021-01959-x PMID:33941231

27. Wang Y, Gao W, Shi X, Ding J, Liu W, He H, Wang K, Shao F. Chemotherapy drugs induce pyroptosis through caspase-3 cleavage of a gasdermin. Nature. 2017; 547:99–103. https://doi.org/10.1038/nature22393 PMID:28459430

28. Jia Y, Cui R, Wang C, Feng Y, Li Z, Tong Y, Qu K, Liu C, Zhang J. Metformin protects against intestinal ischemia-reperfusion injury and cell pyroptosis via TXNIP-NLRP3-GSDMD pathway. Redox Biol. 2020; 32:101534. https://doi.org/10.1016/j.redox.2020.101534 PMID:32330868

29. Luo T, Zhou X, Qin M, Lin Y, Lin J, Chen G, Liu A, Ouyang D, Chen D, Pan H. Corilagin Restrains NLRP3 Inflammasome Activation and Pyroptosis through the ROS/TXNIP/NLRP3 Pathway to Prevent Inflammation. Oxid Med Cell Longev. 2022; 2022:1652244. https://doi.org/10.1155/2022/1652244 PMID:36299604

30. Agarwal A, Gupta S, Sharma R. Oxidative stress and its implications in female infertility - a clinician's perspective. Reprod Biomed Online. 2005; 11:641–50. https://doi.org/10.1016/s1472-6483(10)61174-1 PMID:16409717

31. Wang S, Zheng Y, Li J, Yu Y, Zhang W, Song M, Liu Z, Min Z, Hu H, Jing Y, He X, Sun L, Ma L, et al. Single-Cell Transcriptomic Atlas of Primate Ovarian Aging. Cell. 2020; 180:585–600.e19. https://doi.org/10.1016/j.cell.2020.01.009 PMID:32004457

32. Zeng Y, Qin Q, Li K, Li H, Song C, Li Y, Dai M, Lin F, Mao Z, Li Q, Long Y, Fan Y, Pan P. PKR suppress NLRP3-pyroptosis pathway in lipopolysaccharide-induced acute lung injury model of mice. Biochem Biophys Res Commun. 2019; 519:8–14. https://doi.org/10.1016/j.bbrc.2019.08.054 PMID:31474337